Above- and below-threshold high-order-harmonic generation of H_{2}^{+} in intense elliptically polarized laser fields

K. Nasiri Avanaki, Dmitry A. Telnov, and Shih-I Chu

Exploration of the Above- and Below- Threshold High-Order Harmonic Generation of H_2^+
in Intense Elliptically Polarized Laser Fields

K. Nasiri Avanaki[1], Dmitry A. Telnov[2], Shih-I Chu[1]

[1] Department of Chemistry, University of Kansas, Lawrence, Kansas 66045

[2] Department of Physics, St. Petersburg State University, St.Petersburg 198504, Russia

ABSTRACT

We present an *ab initio* 3D precision calculation and analysis of high-order harmonic generation (HHG) of the hydrogen molecular ion subject to intense elliptically polarized laser pulses by means of the time-dependent generalized pseudospectral (TDGPS) method in two-center prolate spheroidal coordinates. The calculations are performed for the ground and first excited electronic states of H_2^+ at the equilibrium internuclear separation $R = 2$ a.u. as well as for the stretched molecule at $R = 7$ a.u. The spectral and temporal structures of the HHG signal are explored by means of the wavelet time-frequency analysis. Several novel ellipticity-dependent dynamical behaviors are uncovered. We found that the production of above-threshold harmonics for non-zero ellipticity is generally reduced, as compared with LP fields. However, below-threshold harmonics still appear quite strong except when the polarization plane is perpendicular to the molecular axis. Weak even harmonics are detected in the HHG spectra of stretched molecules. This effect can be explained by the broken inversion symmetry due to dynamic localization of the electron density near one of the nuclei. Multiphoton resonance and two-center interference effects are analyzed for the exploration of the quantum origin of the predicted HHG spectral and dynamical behavior.

I. INTRODUCTION

The study of the high harmonic generation (HHG) dynamics and spectroscopy in intense laser fields is one of the forefront topics in ultrafast science and technology [1, 2]. Most of the studies so far have been focused on the use of linearly polarized (LP) laser fields, where the semiclassical 3-step model [3, 4] can provide qualitative understanding of the underlying processes. The use of elliptically polarized (EP) laser fields opens a new direction access to strong-field atomic, molecular, and optical (AMO) and chemical processes that are either hindered or not present under the linear polarization. Earlier study of HHG spectrum in EP fields showed that the HHG yield is decreased with increasing ellipticity [5, 6]. There have been also extensive studies of the polarization properties of HHG generated in atomic gases [7, 8]. For the last decade, HHG has become the most important method for generating the extreme ultraviolet (XUV) attosecond pulses from intense infrared lasers [2, 9]. Since the HHG yield is sensitive to driving laser ellipticity, it has been found recently that the EP light can be used for the generation of isolated attosecond pulses via polarization gating [10]. The study of HHG in EP laser pulses is thus of considerable current interest both theoretically and experimentally [11, 12]. For the molecular systems, the extra internuclear degree of freedom

and the ellipticity of the laser field provide extra control parameters for laser-molecule interactions and introduce some novel features in strong-field HHG processes. However, these extra degrees of freedom also pose considerable challenge for the accurate theoretical and computational study.

In this paper, we perform for the first time a fully *ab initio* 3D and accurate investigation of the effect of ellipticity on the HHG dynamics and spectroscopy of H_2^+ molecules below- and above- the ionization threshold. We show that the generation mechanism of HHG in EP light is considerably different from that in the LP light. Further, in the EP case, particular attention must be paid to follow closely the subtle electron dynamics on the sub-femtosecond time scale and the delicate generation mechanism of HHG below- and above- the ionization threshold. The novel features of HHG in EP light are presented and their quantum origins are explored in details.

The organization of this paper is as follows. In Sec. II, we briefly describe the method that we use for solving the time-dependent Schrödinger equation in prolate spheroidal coordinates and discuss how we calculate the HHG spectra from the time-dependent wave function. In Sec. III, we present our results regarding HHG of the ground and first excited electronic states of H_2^+ in three different cases. The resonance and two-center interference effects in the HHG spectra are discussed in details. Particular attention is paid to the exploration of the fine structures of spectral and time profiles of HHG which provide us with new physical insights regarding the underlying mechanisms for harmonic generation in different energy regimes. Section IV contains concluding remarks.

II. THEORY AND NUMERICAL TECHNIQUES

The simplest diatomic molecule, hydrogen molecular ion H_2^+, has been treated many times previously to study various multiphoton processes in strong laser fields but it still remains an important proto-type system for the investigation of the novel elliptical field effects in HHG of diatomic molecules. In order to get high precision electronic structure results with the use of only a modest number of grid points, we apply the two-center time-dependent generalized pseudospectral (TDGPS) scheme in prolate spheroidal coordinates for accurate and efficient treatment of the time-dependent Schrödinger equation (TDSE) for diatomic molecular systems. The methodology for the HHG calculation starts with solving TDSE in prolate spheroidal coordinates, which are convenient for describing two-center problems. Here we briefly outline the method. Detailed numerical procedures can be found in Ref. [13,14]. The time-dependent electron wave function $\Psi(\boldsymbol{r},t)$ of H_2^+ at a fixed internuclear distance satisfies TDSE (atomic units $\hbar = m = e = 1$ are used unless stated otherwise):

$$i\frac{\partial}{\partial t}\Psi(\boldsymbol{r},t) = \left[H_0(\boldsymbol{r}) + V_{ext}(\boldsymbol{r},t) \right]\Psi(\boldsymbol{r},t), \tag{1}$$

Here H_0 is the unperturbed electronic Hamiltonian:

80
$$H_0(\boldsymbol{r}) = -\frac{1}{2}\nabla^2 + U(\xi,\eta), \tag{2}$$

81 $U(\xi,\eta)$ being the Coulomb interaction with the nuclei (the charge of each center is unity):

82
$$U(\xi,\eta) = -\frac{2\xi}{a(\xi^2 - \eta^2)}. \tag{3}$$

83 Here a is a half internuclear separation; the nuclei are located at the points $-a$ and a on the z-
84 axis. The prolate spheroidal coordinates ξ,η, and φ are related to Cartesian coordinates x, y, and
85 z as follows:

86
$$x = a\sqrt{(\xi^2-1)(1-\eta^2)}\cos(\varphi), \tag{4}$$

87
$$y = a\sqrt{(\xi^2-1)(1-\eta^2)}\sin(\varphi), \tag{5}$$

88
$$z = a\xi\eta \quad (1 \leq \xi < \infty, \; -1 \leq \eta \leq 1). \tag{6}$$

89 The initial wave function represents an eigenstate and can be obtained by solving the unper-
90 turbed eigenvalue problem:

91
$$H_0\Psi(\xi,\eta,\varphi) = E\Psi(\xi,\eta,\varphi). \tag{7}$$

92

93 In Eq. (1), $V_{ext}(t)$ is the term due to the coupling to the external field. We assume that the laser
94 field is EP in the x–z plane:

95
$$\boldsymbol{f}(t) = f_0(t)(\frac{\varepsilon}{\sqrt{1+\varepsilon^2}}\hat{\boldsymbol{e}}_x\cos(\omega_0 t) + \frac{1}{\sqrt{1+\varepsilon^2}}\hat{\boldsymbol{e}}_z\sin(\omega_0 t)). \tag{8}$$

96 Here ε is the ellipticity parameter and ω_0 is the carrier frequency. Then using the dipole approx-
97 imation and the length gauge, we can write the interaction potential $V_{ext}(\xi,\eta,t)$ in the following
98 form:

99
$$V_{ext}(\boldsymbol{r},t) = \boldsymbol{r}.\boldsymbol{f}(t) = af_0(t)\{\frac{\varepsilon}{\sqrt{1+\varepsilon^2}}\sqrt{(\xi^2-1)(1-\eta^2)}\cos(\varphi)\cos(\omega_0 t) + \frac{1}{\sqrt{1+\varepsilon^2}}\xi\eta\sin(\omega_0 t)\}. \tag{9}$$

100 In our calculations, we use the sine-squared pulse shape, and the function $f_0(t)$ can be written
101 as follows:

102
$$f_0(t) = f_0\sin^2\left(\frac{\pi t}{NT}\right), \tag{10}$$

103 where f_0 is the peak field strength, $T = 2\pi/\omega_0$ is the duration of one optical cycle, and N is the
104 number of optical cycles in the pulse.
105 Since H_0 has a rotational symmetry with respect to the molecular axis, the unperturbed initial
106 wave function can be written as

107
$$\Psi(\xi,\eta,\varphi) = \psi_m(\xi,\eta)\exp(im\varphi), \tag{11}$$

3

108 where m is the projection of the electron orbital angular momentum onto the molecular axis. The
109 generalized pseudospectral method [14, 15] is employed to discretize ξ, η and propagate the
110 time-dependent wave function in the energy representation using the second-order split-operator
111 method according to

112 $$\Psi(r, t + \Delta t) \approx \exp\left(-i\frac{\Delta t}{2} H_0(r)\right) \exp\left(-i\Delta t V\left(\xi, \eta, t + \frac{1}{2}\Delta t\right)\right) \exp\left(-i\frac{\Delta t}{2} H_0(r)\right) \Psi(r, t) + O(\Delta t^3).$$

113 (12)

114

115 Once the wave function is computed, we can proceed to calculate the spectra of the emitted high-
116 order harmonic radiation. To calculate the HHG spectra, we employ the widely-used semiclas-
117 sical approach, replacing the classical quantities with the corresponding quantum expectation
118 values. The spectral density of the radiation energy emitted for all the time is given either by the
119 length form

120 $$S(\omega) = \frac{2\omega^4}{3\pi c^3} |D_\omega|^2,$$ (13)

121 or acceleration form

122 $$S(\omega) = \frac{2}{3\pi c^3} |A_\omega|^2,$$ (14)

123 D_ω and A_ω are the Fourier transforms of the time-dependent dipole moment and acceleration,
124 respectively:

125 $$D_\omega = \int_{-\infty}^{\infty} dt D(t) \exp(i\omega t),$$ (15)

126

127 $$A_\omega = \int_{-\infty}^{\infty} dt A(t) \exp(i\omega t).$$ (16)

128 The time-dependent dipole moment and acceleration are evaluated as expectation values with the
129 time-dependent wave function $\Psi(\xi, \eta, \varphi, t)$

130 $$D(t) = \langle \Psi | r | \Psi \rangle,$$ (17)

131 $$A(t) = -\langle \Psi | \nabla U | \Psi \rangle - f(t),$$ (18)

132 By adjusting the numerical parameters of the present calculations such as the number of grid
133 points, the box size, and absorber position, we reproduce the ground state and low-lying excited
134 states energies of H_2^+ with the machine accuracy. To achieve convergence of the computed HHG
135 spectra for the laser field parameters and internuclear separations used in the calculations (see
136 Sec. III below), we set the number of grid points to 160 and 48 for the ξ and η coordinates, re-
137 spectively, and include the angular momentum projections -24 to 24. For the time propagation,
138 we use 4096 time steps per optical cycle (81920 steps for the whole pulse of 20 optical cycles).
139 To accommodate all important physics in the laser field, the linear dimension of the box is cho-

140   sen at 60 a.u. In the layer between 40 a.u. and 60 a.u., we place an absorber which prevents spu-

141   rious reflections of the wave packet from the grid boundary. Our numerical scheme and selec-

142   tion of the parameters secure the accuracy of the results obtained. In the calculations of the HHG

143   spectra, we use the length form (15); the acceleration form provides almost identical results, in-

144   dicating a good quality of our wave functions.

145

146

147   **III. RESULTS AND DISCUSSION**

148   We have performed the calculations of HHG spectra emitted by H_2^+ in $1\sigma_g$ and $1\sigma_u$ elec-

149   tronic states in an intense EP laser field. In all cases we used a 20- optical cycles laser pulse with

150   the sine-squared envelope, the carrier wavelength 800 nm (corresponding to the photon energy

151   1.55 eV), and the peak intensity 2×10^{14} W/cm^2. According to the well-known atomic recollision

152   model [3], the HHG spectra should present a plateau region with a cutoff at the energy

153    $|I_P| + 3.17 U_P$ where $|I_P|$ is the ionization energy of the initial state and Up is the ponderomo-

154   tive potential (for the LP laser field, $U_P = I^2 / (4\omega_0^2)$, I being the laser intensity). For diatomic

155   molecules, the collision with the parent core resembles the single atom case and leads to the

156   same harmonic spectrum cutoff position independent of the laser field intensity and internuclear

157   separation. However, there is a possibility of collision with the other nucleus. In the latter case,

158   the field intensity and frequency as well as the distance between the nuclei can affect the return

159   kinetic energy of the electron [16]. The vertical ionization potential I_P of H_2^+ is equal to 30 eV

160   for the $1\sigma_g$ state and 18 eV for the $1\sigma_u$ state, at the equilibrium internuclear separation of 2 a.u.

161   Then the cutoff corresponds to the harmonic orders 43 and 36, respectively.

162

163   **HHG spectra of H_2^+ in $1\sigma_g$ electronic state**

164

165   Fig.1(a) shows the HHG spectral density of H_2^+ for $1\sigma_g$ electronic state with different ellip-

166   ticity parameters. As one can see, the semiclassically predicted cutoff positions are in fair agree-

167   ment with our calculations in the LP filed. Generally, elliptical polarization (and circular polari-

168   zation to more extent) will reduce the probability of recollision and thus reduce the intensity of

169   above-threshold harmonics (that is harmonics with the photon energies above the ionization thre-

170   shold). The intensity of below-threshold harmonics (harmonics with the photon energies below

171   the ionization threshold) is also reduced because the dipole transitions are forbidden if the angu-

172   lar momentum projection m is changed more than by unity (and each absorbed circularly pola-

173   rized photon increases m by 1). All this is true for atoms in laser fields. For molecules, the pic-

174   ture is different: first, due to broken spherical symmetry and m selection rule; second, because

175   the recollision can take place not only on the parent nucleus but also on the other nucleus. Our

176   results demonstrate specific difference between the atoms and molecules. As expected, the HHG

177 cutoff position is shifted to lower frequencies as the ellipticity parameter increases from 0 (linear
178 polarization) to 1 (circular polarization). Interestingly, just a few of the lower harmonics show up
179 in the circularly polarized (CP) filed. Comparing the intensity of the harmonics in different cases
180 $(\varepsilon = 0, 0.5, 1)$ presented in Fig. 1(a), we can see that the intensities of lower-order harmonics are
181 comparable. However, as we go to higher harmonics, their intensities in the EP and CP fields
182 decrease by several orders of magnitude with respect to the linear polarization case. Looking
183 carefully at Fig.1(b), one can notice the peaks at the harmonic orders 7.65 and 11.65, which do
184 not correspond to odd integer numbers. Based on the unperturbed electronic energy values of
185 H_2^+, we attribute the first peak, located near the 7th harmonic (harmonic order 7.65), to the re-
186 sonance with the first excited ($1\sigma_u$) state. Accordingly, the second peak, which appears close to
187 the 11th harmonic (harmonic order 11.65), is attributed to the resonance with the second excited (
188 $1\pi_u$) state. We note that the first resonance peak shows up in the HHG spectrum irrespectively
189 of the ellipticity parameter, while the second resonance is absent in the linear polarization case
190 $(\varepsilon = 0)$. This is well explained by the dipole selection rules: transitions between   and   states
191 are forbidden when the external field is directed along the molecular axis.
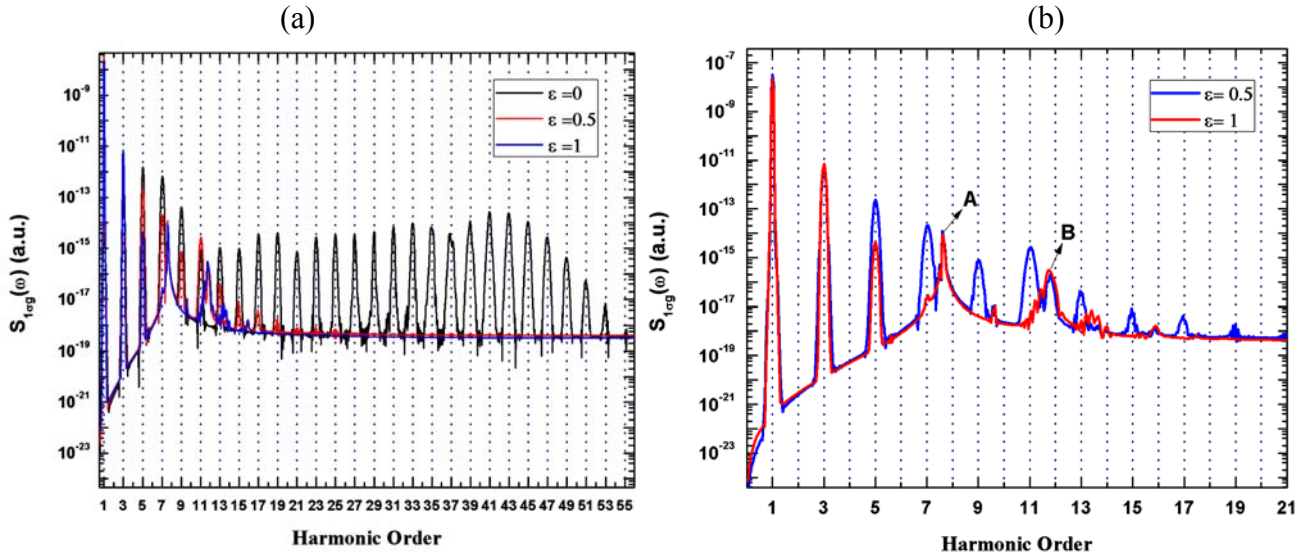192

(a)   (b)

Fig.1. (Color online) panel(a) shows the HHG spectrum $S(\omega)$ from $1\sigma_g$ state of H_2^+ at $R = 2$ a.u. in the laser field with
$\lambda = 800$ nm and peak intensity 2×10^{14} W/cm^2 for different ellipticity parameters $(\varepsilon = 0, 0.5, 1)$. Panel (b) demonstrates
resonance structures for $(\varepsilon = 0.5, 1)$ near 7th and 11th harmonics. Arrows mark the resonance peaks in the spectrum in CP
field. Resonance A corresponds to excitation of $1\sigma_u$ state, resonance B is due to coupling to $1\pi_u$ state.

193
194   To explore the detailed spectral and temporal structure of HHG and the underlying me-
195 chanisms in different regimes, we perform the time-frequency analysis by means of the wavelet
196 transform [17,18] of the induced dipole,

197
$$d_{\omega}(t_0) = \int D(t) W_{t_0,\omega}(t) dt, \tag{19}$$

198   with the wavelet kernel $W_{t_0,\omega}(t) = \sqrt{\omega} W(\omega(t-t_0))$ For the harmonic emission, a natural choice

199   of the mother wavelet is given by the Morlet wavelet [18]:

200
$$W(x) = \left(\frac{1}{\sqrt{\tau}}\right) e^{ix} \exp(\frac{-x^2}{2\tau^2}) . \tag{20}$$

201   Here the wavelet window function varies with the frequency but the total number of oscillations
202   (proportional to τ) within the window is fixed, however in the Gabor transform [18] the width of
203   the window function is held constant. For the calculations discussed below, we choose $\tau = 15$ to
204   perform the wavelet transform.
205   In Figs. 2(a, b), we show the absolute value of the time-frequency spectrum $|d_{\omega}(t)|$ for
206   the $1\sigma_g$ state of H_2^+ at $R = 2$ a.u. in laser fields with peak intensity $2\times10^{14}\,W/cm^2$ and elliptici-
207   ty parameters $(\varepsilon = 0)$ and $(\varepsilon = 0.5)$. The $1\sigma_u$ resonance is clearly seen at the harmonic order
208   7.65 in both LP and EP fields, while the $1\pi_u$ resonance shows up at the harmonic order 11.65 in
209   the case of elliptical polarization only.
210

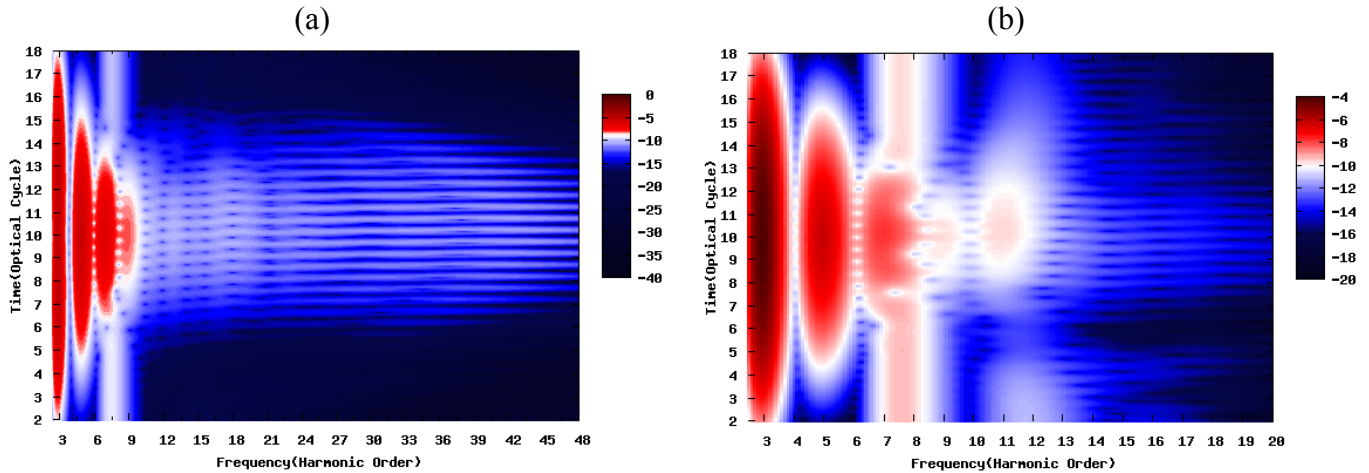(a)   (b)

Fig.2. (Color online) Time-frequency spectra for $1\sigma_g$ state of H_2^+ at $R = 2$ a.u. in the field with $\lambda = 800$ nm and peak intensity
2×10^{14} W/cm^2 for different ellipticity parameters $\varepsilon = 0$ in panel (a) and $\varepsilon = 0.5$ in panel (b). The color scale is logarithmic.

211

212   The cross section of the time-frequency profile corresponding to a specific harmonic order
213   yields a function of time which exhibits a different pattern depending on the harmonic order. For
214   the lowest few harmonics and all ellipticities that we study here, we obtain a smooth function,
215   which resembles the envelope of the driving laser pulse. This is a manifestation of the dominant
216   multiphoton mechanism in lower harmonic regime. In this regime, the probability of absorbing
217   of N photons is about I^N (I is the laser intensity and proportional to $[f(t)]^2$). In this part of the
218   HHG spectrum, the smooth time profile becomes narrower as the harmonic order is increased. In
219   the frequency domain, the corresponding frequency profile becomes wider (see Fig. 2). As the

7

220 harmonic order is further increased in the below-threshold region, the time profiles develop
221 spread fine structures, which resemble the pattern for the above-threshold harmonics and may be
222 attributed to the effect of the quasi-continuum formed by highly excited bound states.

223   For higher harmonics above the ionization threshold, the time profiles manifest multiple
224 bursts, with two bursts per optical cycle. Each burst is due to the recollision of the electronic
225 wave packet with the ionic core. Transformation of the time-frequency spectra with increasing
226 harmonic order is well illustrated by Fig. 2.

227   One can see that the (multiphoton-dominant) low-order harmonics form *continuous time*
228 *profiles* at a given frequency. However, for higher harmonic orders, the tunneling-recollision
229 mechanism becomes dominant, and the time-frequency profiles show a netlike structure. This
230 structure is more pronounced for the LP field (Fig. 2(a)) than in the case of elliptical polarization
231 (Fig.2(b)). This is well understood since the recollision becomes increasingly suppressed when
232 the ellipticity parameter increases.

233   We have also performed calculations on stretched H_2^+ molecules with the internuclear se-
234 paration $R = 7$ a.u. The HHG spectra $S(\omega)$ are shown in Fig.3(a-b). The two lowest electronic
235 states, $1\sigma_g$ and $1\sigma_u$, become nearly degenerate at larger R (at $R = 7$ a.u., their vertical ionization
236 potentials are 17.6 eV and 17.4 eV, respectively). In the presence of the external fields, the elec-
237 tric dipole coupling of $1\sigma_g$ and $1\sigma_u$ is proportional to R and becomes very significant. This phe-
238 nomenon, known as the ''charge resonance'' (CR) effect, takes place only in the odd-charged
239 molecular-ion systems. In LP fields, the combined effect of CR and the multiphoton transitions
240 to excited electronic states is the main mechanism responsible for the enhanced ionization phe-
241 nomenon [19]. Compared with the case $R = 2$ a.u., the ionization probability of H_2^+ is greatly
242 increased due to reduced ionization potential in stretched molecules at $R = 7$ a.u. (the minimum
243 number of photons required for ionization of the $1\sigma_g$ state is equal to 11 compared to 20 at $R = 2$
244 a.u.). According to the three-step model [16], it leads to enhancement in HHG, resulting in more
245 intense signal and appearance of more distinct harmonics in the high-energy region of the spec-
246 trum (see Fig.3(b)).

247 The HHG spectra in Fig.3 (a) for LP and EP fields exhibit several maxima and minima that can
248 be related to the two-center nature of diatomic molecules [20] (see also discussion in Refs.
249 [14,21]). Since the returning electron can experience a recollision at any nucleus, the contribu-
250 tions to the recombination amplitude from both nuclei are added coherently, giving rise to the
251 interference structure in the HHG spectra. Using a simple recollision model, one can easily ob-
252 tain the interference minima or maxima positions in the case of LP fields [20]:

$$\cos\alpha = \frac{n\pi}{R\sqrt{2E_{ke}}} \qquad n = 1, 2, 3... \tag{21}$$

254 where E_{ke} is the kinetic energy of the recolliding electron, α is the angle between the polariza-
255 tion vector of the laser field and the molecular axis, and R is the distance between the two cen-
256 ters (that is, internuclear distance for diatomic molecules).

257   Assuming all the kinetic energy of the electron is transformed into the harmonic radiation energy
258   during the recollision ($E_{ke} = N_h\omega_0$, where N_h is the harmonic order), for the laser field paral-
259   lel to the molecular axis (cosα=1), and for the given internuclear separation R and laser frequen-
260   cy ω_0, one can obtain the harmonic order N_h where the minimum or maximum should be lo-
261   cated. For the $1\sigma_g$ state, $n = 1,3,5...$ in Eq.(21) correspond to a minimum, and $n = 2,4,6...$ cor-
262   respond to a maximum. Thus a simple calculation can give us an estimate of the harmonic order
263   where the interference maxima or minima are expected in the HHG spectrum. For H_2^+ at the in-
264   ternuclear separation $R = 7$ a.u. subject to the 800 nm LP laser field, only the first few minima
265   and maxima can be relevant for the two-center interference analysis of the HHG spectrum. For
266     $n = 3$ and $n = 5$, the minima can be expected at the harmonic orders 16 and 44, respectively.
267   The maxima for $n = 2,4,6$ can be found around the harmonic orders 7, 28 and 63. These posi-
268   tions are marked in Fig.3(a) with blue circles. Except the maximum at the harmonic order 28, the
269   other predictions are in fair agreement with our calculations. We should note that Eq. (21)
270   represents a rough model and is derived in the case of linear polarization; for EP fields, the esti-
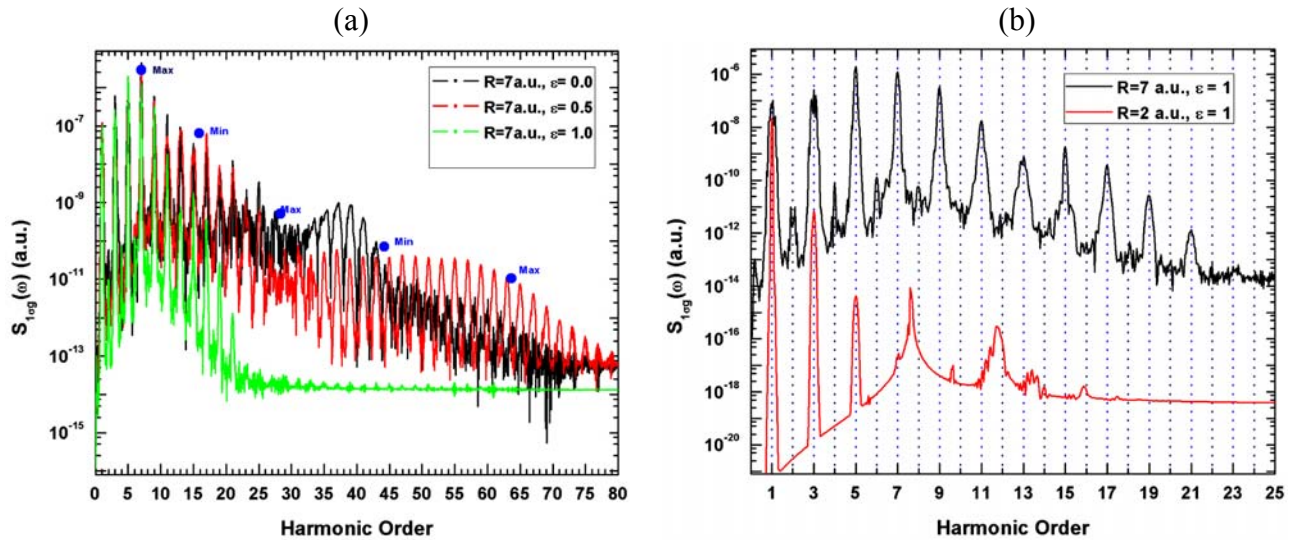271   mates based on this equation become even less accurate.

Fig 3. (Color online) HHG spectra $S(\omega)$ from $1\sigma_g$ state of H_2^+ at $R = 7$ a.u. in the laser field with $\lambda = 800$ nm and peak intensity 2×10^{14} W/cm^2 (a) HHG spectra for different ellipticity parameters $(\varepsilon = 0.5,1)$. (b) Comparison of HHG spectra for the same laser field parameters for CP at $R = 7$ a.u. and $R = 2$ a.u.

272
273   At the internuclear separation $R = 7$ a.u., a comb of well-resolved odd- and even-order harmonics,
274   particularly in the lower energy part of the HHG spectra, is observed. The odd harmonics are at
275   least four orders of magnitude stronger than the even harmonics (see Fig. 3(b) where the spectra
276   at $R = 2$ a.u. and $R = 7$ a.u. are compared in the case of CP field). By varying numerical simula-
277   tion parameters such as the number of grid points, the box size, and the absorber position, we
278   have confirmed that the results are converged and existence of even harmonics cannot be attri-

279 buted to numerical inaccuracy. This is surprising since one would not normally expect generation
280 of even harmonics from homonuclear diatomic molecules. Generally, generation of even har-
281 monics is forbidden by a fundamental symmetry, which combines the inversion symmetry of the
282 media and the half-wave symmetry of the driving field. Thus in atoms, the presence of only odd
283 harmonics are an indication of the spatial inversion symmetry of the electron–atom interaction
284 energy [22, 23]; the same is true for homonuclear diatomic molecules. It is proven that if *hetero-*
285 *nuclear* diatomic molecules in the gas are oriented [24] or if the half-wave symmetry of the driv-
286 ing field is broken [25], then the HHG spectrum consists of both odd and even harmonics. Strict-
287 ly speaking, if the driving field represents a pulse but not a continuous wave, the half-wave
288 symmetry is broken, and generation of even harmonics is possible. However, this effect is neg-
289 ligible for long enough pulses. Indeed, for the pulse duration of 20 optical cycles, we do not see
290 even harmonics at the internuclear distance $R = 2$ a.u., but those harmonics do appear at $R = 7$ a.u.
291 We explain this phenomenon by the effect of a dynamical rupture of symmetry (DRS) [26,27].
292 The idea behind DRS is that the electron, initially symmetrically distributed over the two nuclei,
293 becomes essentially localized over one of the nuclei, and periodically bounces back and forth
294 from nucleus to nucleus. During the confinement time over one of the two nuclei, the electron
295 experiences a non-symmetric potential, which is the sum of the symmetric atomic potential of
296 the near nucleus plus the tail of the potential of the far nucleus; this DRS causes the emission of
297 even harmonics [26,27]. For H_2^+ at the internuclear separation $R = 7$ a.u., the DRS effect is en-
298 hanced by existence of the CR states. In the laser field with the intensity as high as 2×10^{14}
299 W/cm², a significant amount of the electron population is transferred from the initial $1\sigma_g$ state to
300 the $1\sigma_u$ state, resulting in a non-symmetric electron density distribution.
301
302
303 **b) HHG spectra of H_2^+ in $1\sigma_u$ electronic state**
304 We have also performed the calculations of the HHG spectra emitted by H_2^+ in the $1\sigma_u$ (first
305 excited) electronic state. The parameters of the laser pulse are the same as in the previous calcu-
306 lations at $R = 2$ a.u. Fig.4 (a) displays the HHG spectra of H_2^+ for the $1\sigma_u$ electronic state with
307 different ellipticity parameters $\varepsilon = 0, 0.5, 1$. We can see that the HHG cutoffs are shifted to lower
308 energies as the ellipticity parameter increases from linear to circular polarization, in agreement
309 with general predictions for EP laser fields. It appears that the HHG signal for the initial $1\sigma_u$
310 state is several orders of magnitude stronger than that for the $1\sigma_g$ state, with the same laser pulse
311 parameters, as one can see from Fig.4(a,b). This is well explained by much lower ionization po-
312 tential (and, hence, much higher ionization probability) of the $1\sigma_u$ state at the internuclear sepa-
313 ration $R = 2$ a.u. Analysis of below-threshold harmonics (the minimum number of photons re-
314 quired for ionization is 12 while the cutoff is around harmonic order 36) in the cases $\varepsilon = 0.5$
315 and $\varepsilon = 1$ (Fig.4(b)) reveals resonance peaks in the vicinity of the 5th and 7th harmonics. The
316 unperturbed bound state energies of H_2^+ suggest that the first peak, which appears near the 5th

317 harmonic, corresponds to the resonance with the $2\sigma_g$ state. As to the second peak, located near

318 the 7th harmonic, it can be attributed to the resonances with the $1\sigma_g$, $3\sigma_g$, and $1\pi_g$ states. These

319 resonances are not resolved into separate peaks since their transition energies are very close to

320 each other.

321   Since the diatomic molecule H_2^+ does not possess the spherical symmetry, the effect of EP

322 laser field depends on the orientation of the molecular axis with respect to the polarization plane

323 of the field. Above we have studied one representative case, when the molecular axis lies in the

324 polarization plane and is directed along the major axis of the polarization ellipse. Now we con-

325 sider another important case, when the molecular axis is perpendicular to the polarization plane

326 (that is, the field is polarized in the x-y plane):

327
$$\boldsymbol{f} = f_0(t)\left(\frac{\varepsilon}{\sqrt{1+\varepsilon^2}}\hat{e}_x \cos(\omega_0 t) + \frac{1}{\sqrt{1+\varepsilon^2}}\hat{e}_y \sin(\omega_0 t)\right), \tag{22}$$

328
$$V_{ext}(t) = \boldsymbol{r}.\boldsymbol{f} = af_0 \sin^2\left(\frac{\pi t}{nT}\right)\sqrt{(\xi^2-1)(1-\eta^2)}\{\frac{\varepsilon}{\sqrt{1+\varepsilon^2}}\cos(\varphi)\cos(\omega_0 t)$$
$$+ \frac{1}{\sqrt{1+\varepsilon^2}}\sin(\varphi)\sin(\omega_0 t)\}, \tag{23}$$

329 Here we report the results regarding the circular polarization (e =1) only. For the polarization in

330 the x-y plane, the situation resembles the atomic case since the same selection rules apply to the

331 angular momentum projection onto the axis perpendicular to the polarization plane (that is, the

332 molecular axis). For the unperturbed molecule, the angular momentum projection m on the mo-

333 lecular (z) axis is conserved. In the CP field in the x-y plane, absorption of each photon changes

334 this projection by $\Delta m = 1$ or $\Delta m = -1$ for the right and left polarization, respectively. Thus

335 absorption of several photons from the field leads to population of the states with large m values;

336 dipole transitions from such states to the ground state with emission of a single photon are for-

337 bidden by the selection rules. In Fig.4(b), we can see strong suppression of HHG for both below-

338 threshold and above-threshold harmonics. For the polarization in the x-z plane, the situation is

339 different: the HHG is suppressed but not that much as in the x-y polarization case. Moreover, the

340 below-threshold harmonics are quite strong, and this happens because there is no $\Delta m = \pm 1$ se-

341 lection rule (for each absorbed photon) with respect to the molecular axis.
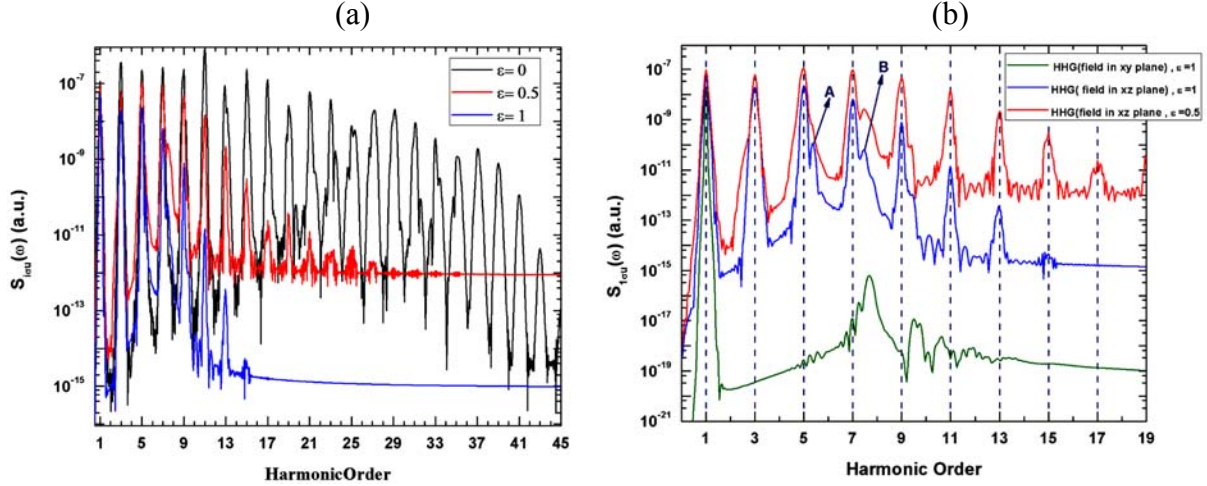
342

343

344

345

346

347

348

349

350

351

(a)   (b)

Fig.4. (Color online) HHG spectra $S(\omega)$ from $1\sigma_u$ state of H_2^+ at $R = 2$ a.u. in the laser field with $\lambda = 800$ nm and peak intensity 2×10^{14} W/cm^2 (a) HHG spectra for the field polarized in x-z plane and $(\varepsilon = 0, 0.5, 1)$. (b) HHG spectra for $\varepsilon = 0.5, 1$ with resonance structures near the 5th and 7th harmonics. The arrows mark the resonance peaks in the spectrum. Resonance A corresponds to excitation of $2\sigma_g$ state, resonance B is due to coupling to $1\sigma_g$, $3\sigma_g$, and $1\pi_g$ states. Also shown is the HHG spectrum for the CP field in x-y plane.

352   To illustrate the mechanisms of HHG in the $1\sigma_u$ state of H_2^+, we perform a time-
353   frequency analysis and plot the time-frequency spectrum $|d_\omega(t)|$ for the case of circular polari-
354   zation in the x-z plane (Fig.5). One can clearly see the resonances near the 5th and 7th harmonics;
355   the resonance lines remain quite strong even at the end of the pulse, when the external field va-
356   nishes. The HHG mechanisms are revealed by the time profiles of the harmonics in different
357   energy regions obtained by performing the cross section of the time-frequency spectrum. For the
358   lowest few harmonics, the time profile (at a given frequency) shows a smooth function corres-
359   ponding to the envelope of the driving laser pulse. This behavior resembles what we obtain for
360   the $1\sigma_g$ state and manifests the dominant multiphoton mechanism in the low energy region.

361   Development of extended fine structures in the time profiles of the higher harmonic or-
362   der can be attributed to the effect of excited states and the onset of the continuum. In the inter-
363   mediate energy regime, where both multiphoton and tunneling mechanisms contribute, the time-
364   frequency profiles show a netlike structure, as seen in Fig.5. Since the HHG spectrum in the cir-
365   cular polarization case is quite short, and there is no clear plateau well above the ionization thre-
366   shold, the fast burst time profiles corresponding to the tunneling regime are developed by a few
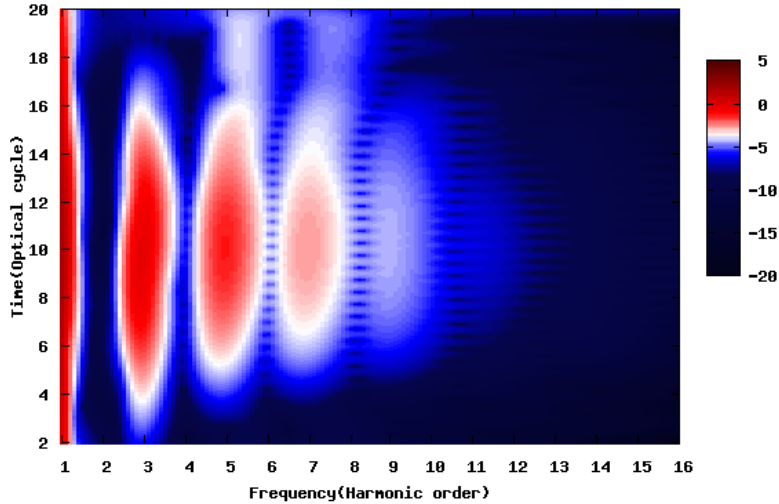367   harmonic only.

368

Fig.5 (Color online) Time-frequency spectra for $1\sigma_u$ state of H_2^+ at $R = 2$ a.u. in the field with $\lambda = 800$ nm, peak intensity 2×10^{14} W/cm^2, and the ellipticity parameter $\varepsilon = 1$ The color scale is logarithmic.

IV. CONCLUSION

In conclusion, we have presented *ab initio* high-precision study of high-order harmonic generation of the hydrogen molecular ion in intense laser fields. It is found that the HHG yield is very sensitive to the ellipticity of the driving laser field. The reduction in the production of above-threshold harmonics for non-zero ellipticity, particularly for $\varepsilon = 0.5$ and $\varepsilon = 1$ is partially explained by the third step of the recollision model: the transverse component of the laser field tilt the trajectory of the electron and prevent it from recombining with the parent nucleus (it may recombine with the other nucleus, however). If the polarization plane of the laser field contains the molecular axis, the below-threshold harmonics still appear quite strong, even for circular polarization, in contrast with the case when the polarization plane is perpendicular to the molecular axis. This happens because the excited bound states with the angular momentum projections $m = 0$ and $m = 1$ onto the molecular axis (that is, σ and π states) still can be populated by absorption of multiple photons in the CP field, provided the molecular axis has a non-zero projection in the polarization plane. These excited states then allow transitions to the ground state with emission of a single photon.

Such multiphoton excitations followed by transitions to the ground state with emission of a single photon are not permitted for atoms since atomic states possess definite angular momentum, which must increase by one after absorption of each CP photon. Thus the reduced symmetry of diatomic molecules, as compared with atoms, leads to qualitative differences between the atomic and molecular HHG spectra in EP laser fields, with higher HHG yield from molecules. Another feature revealed by the present calculations is also related to the reduced symmetry. Weak even harmonics observed in the HHG spectra of H_2^+ molecules stretched at the internuc-

lear distance $R = 7$ a.u. can be explained by dynamically broken inversion symmetry, when the electron density is periodically localized near one of the two nuclei.

The method discussed in the present paper for the one-electron molecular ion H_2^+ can be generalized for multielectron diatomic molecules with the help of the self-interaction-free time-dependent density functional theory [28-30]. For multielectron molecules, commonly used restriction to the highest-occupied molecular orbital may appear insufficient. Correct description of the HHG spectra in this case may require taking into account the inner-shell orbitals as well. Extension of the TDDFT for the study of HHG from multielectron diatomic molecules in EP laser fields is in progress.

REFERENCES

[1]. S. R. Leone et al., Nature Photonics 8, 162 (2014).

[2]. Zenghu Chang and P. Corkum, J. Opt. Soc. Am. B 27, B9 (2010).

[3]. P.B. Corkum, Phys. Rev. Lett. 71, 1994 (1993).

[4]. K. C. Kulander et al., in Super-Intense Laser-Atom Physics,Vol. 316 of NATO Advanced Study Institute Series B: Physics, edited by P. B. Piraux et al. (Plenum, New York, 1993).

[5]. K. S. Budil, P. Salières, A. L'Huillier, T. Ditmire, and M. D. Perry, Phys. Rev. A 48, R3437 (1993).

[6]. Y. Liang, M. V. Ammosov, and S. L. Chin, J. Phys. B 27, 1269(1994).

[7]. J. G. Eden, Prog. Quantum Electron. 28, 197 (2004); 29, 257(E)(2005).

[8]. D. B. Milošević, W. Becker, and R. Kopold, Phys. Rev. A 61, 063403 (2000).

[9]. F. Krausz and M. Ivanov, Rev. Mod. Phys. 81, 163 (2009).

[10]. M. Möller, Y. Cheng, S. D. Khan, B. Zhao, K. Zhao, M. Chini, G. G. Paulus, and Z. Chang, Phys. Rev. A 86, 011401(2012).

[11]. Sabih D. Khan, Yan Cheng, Max Möller, Kun Zhao, Baozhen Zhao, Michael Chini, Gerhard G. Paulus, and Zenghu Chang, Appl. Phys. Lett. 99, 161106 (2011).

[12]. M.V. Frolov, N.L. Manakov, T.S. Sarantseva, and A.F. Starace, Phys. Rev. A **86**, 063406 (2012). M.V. Frolov, N.L. Manakov, T.S. Sarantseva, and A.F. Starace, Phys. Rev. A **86**, 063406 (2012).

[13]. X. Chu and S. I. Chu, Phys. Rev. A 63, 013414 (2000).

[14]. D. A. Telnov and S. I. Chu, Phys. Rev. A 76, 043412 (2007).

[15]. X. M. Tong and S. I. Chu, Chem. Phys. 217, 119 (1997).

[16]. R. Kopold, W. Becker, and M. Kleber, Phys. Rev. A 58, 4022 (1998).

[17]. X. M. Tong and S. I. Chu, Phys. Rev. A 61, 021802 (2000).

[18]. C. K. Chui, An Introduction to Wavelets (Academic Press, New York, 1992).

[19]. Xi Chu and S. I. Chu, Phys. Rev. A 63, 013414 (2000).

[20]. M. Lein, N. Hay, R. Velotta, J. P. Marangos, and P. L. Knight, Phys. Rev. A 66, 023805 (2002).

[21]. D. A. Telnov and S. I. Chu, Phys. Rev. A 80, 043412 (2009).

[22]. M. H. Mittleman, Theory of Laser Atom Interaction (Plenum, New York, 1982).

[23]. F. Martín, J. Fernàndez, T. Havermeier, et al., Science315, 629 (2007).

[24]. E. Frumker, C. T. Hebeisen, N. Kajumba, J. B. Bertrand, H. J.Worner, M. Spanner, D. M. Villeneuve, A. Naumov, and P. B. Corkum, Phys. Rev. Lett. 109, 113901 (2012).

[25]. M. Kozlov, O. Kfir, A. Fleischer, A. Kaplan, T. Carmon, H.G. L. Schwefel, G. Bartal and O. Cohen, New J. Phys.14, 063036 (2012).

[26]. G. Castiglia, P. P. Corso, R. Daniele, E. Fiordilino, F. Morales, and G. Orlando, Laser Physics, 2007, Vol. 17, No. 10, pp. 1240–1245.

[27]. Pietro Paolo Corso, Emilio Fiordilino, Gianfranco Orlando, Franco Persico, Journal of Modern Optics,54,10, 1387-1393(2007)

[28]. X. Chu and S. I. Chu, *Phys. Rev. A* **63**, 023411 (2001)

[29]. D. A. Telnov and S. I. Chu, *Phys. Rev. A* **80**, 043412 (2009)

[30]. J. Heslar, D. A. Telnov, and S.I. Chu, *Phys. Rev. A* **83**, 043414 (2011)